A bi-component model to assess the rheology of soft cellular aggregates probed using the micropipette aspiration technique

Giuseppe Sciumè, Karine Guevorkian, Pierre Nassoy

Acta Biomaterialia 189 (2024) 449–460

Contents lists available at ScienceDirect

Acta Biomaterialia

journal homepage: www.elsevier.com/locate/actbio

Full length article

A bi-component model to assess the rheology of soft cellular aggregates probed using the micropipette aspiration technique

Giuseppe Sciumè[a,b,c,*], Karine Guevorkian[d], Pierre Nassoy[e,f]

[a] University Bordeaux, CNRS, Bordeaux INP, I2M, UMR 5295, F-33400, Talence, France
[b] Arts et Metiers Institute of Technology, CNRS, Bordeaux INP, Hesam Universite, I2M, UMR 5295, F-33400 Talence, France
[c] Institut Universitaire de France (IUF), France
[d] Institut Curie, Université PSL, Sorbonne Université, CNRS UMR168, Physique des Cellules et Cancer, 75005 Paris, France
[e] LP2N, Laboratoire Photonique Numérique et Nanosciences, University Bordeaux, F-33400 Talence, France
[f] Institut d'Optique Graduate School & CNRS UMR 5298, F-33400 Talence, France

ARTICLE INFO

Article history:
Received 25 April 2024
Revised 21 September 2024
Accepted 24 September 2024
Available online 1 October 2024

Keywords:
Phase-field modeling
Viscoelastic rheology
Wettability
Finite element solution

ABSTRACT

The micro-pipette aspiration technique is a classical experiment used to characterize the physical properties of inert fluids and biological soft materials such as cellular aggregates. The physical parameters of the fluid, as viscosity and interfacial tension, are obtained by studying how the fluid enters the pipette when the suction pressure is increased and how it relaxes when the suction pressure is put to zero. A mathematical model representative of the experiment is needed to extrapolate the physical parameters of the fluid-like matter; however, for biological materials as cells or cell aggregates mathematical models are always based on strong starting hypotheses that impact the significance of the identified parameters. In this article, starting from the bi-constituent nature of the cell aggregate, we derive a general mathematical model based of a Cahn–Hilliard–Navier–Stokes set of equations. The model is applied to describe quantitatively the aspiration-retraction dynamics of a cell-aggregate into and out of a pipette. We demonstrate the predictive capability of the model and highlight the impact of the assumptions made on the identified parameters by studying two cases: one with a non-wetting condition between the cells and the wall of the pipette (classical assumption in the literature) and the second one, which is more realistic, with a partial wetting condition (contact angle $\theta_s = 150°$). Furthermore, our results provide a purely physical explanation to the asymmetry between the aspiration and retraction responses which is alternative to the proposed hypothesis of an mechano-responsive alteration of the surface tension of the cell aggregate.

Statement of significance

Our study introduces a general mathematical model, based on the Cahn-Hilliard-Navier-Stokes equations, tailored to model micro-pipette aspiration of cell aggregates. The model accounts for the multi-component structure of the cell aggregate and its intrinsic viscoelastic rheology. By challenging prevailing assumptions, particularly regarding perfect non-wetting conditions and the mechano-responsive alteration of cell surface tension, we demonstrate the reliability of the mathematical model and elucidate the mechanisms at play, offering a purely physical explanation for observed asymmetries between the aspiration and retraction stages of the experiment.

* Corresponding author at: Institute of Mechanics and Mechanical Engineering - I2M, CNRS (UMR 5295), University of Bordeaux, 351, cours de la Libération (Bât. A11) 33405 Talence, France.
E-mail address: giuseppe.sciume@u-bordeaux.fr (G. Sciumè).

https://doi.org/10.1016/j.actbio.2024.09.043

1. Introduction

Mechanical cues contribute to the regulation of a wide range of processes in living systems at different spatial scales [1]. At the molecular scale, mechanobiology aims at deciphering the underlying mechanisms associated to the way cells sense and adapt to the forces exerted by their neighbors through the reinforcement or weakening of adhesive interactions (in the case of catch- and slip-bonds respectively) or to the signals from the surrounding matrix by the alteration of specific biochemical pathways. At the cellular level, shear, stretch, compression, osmotic shock impact the fate of cells, including apoptosis or differentiation, as well as their proliferation, migration, or adhesion. Finally, at the tissue level, externally-applied or internally-generated cues within a tissue such as a spheroid or organoid may direct embryo morphogenesis, cell escape from tumors, and tissue shaping. To apply perturbations in a controlled manner and/or quantitatively assess the forces at play, numerous methodologies and instruments have been developed in the last decades [2,3]. Optical tweezers, magnetic tweezers, single particle tracking rheometry, Atomic Force Microscopy (AFM), Biomembrane Force Probe (BFP) were mostly used in molecular and sub-cellular mechanobiology. At the cellular level several techniques based on microfabricated pillars, microplate rheometry, AFM, single cell micropipette aspiration and magnetic twisting cytometry provide a wealth of information on cellular mechanobiology. At the multicellular scale, tissue surface tensiometry, which yields the surface tension of a multicellular spheroid squeezed between plates [4] and micropipette aspiration (MPA) [5], which consists in partially aspirating a multicellular assembly inside a glass capillary [6,7] are the most employed methods. Historically, the MPA technique was first proposed as a "cell elastimeter" in 1954 [8] before being popularized in particular by E. Evans to measure the shear modulus and membrane viscosity of red blood cells [9], bending rigidity elastic modulus, water permeability and lysis tension of lipid membranes [10,11], cortical tension and apparent tension of granulocytes [12]. From these experiments on individual lipid vesicles and cells using the same technique but different experimental procedures (*e.g.* time-dependent versus steady state) and analyses based on a preliminary knowledge of the cell material, a variety of physical parameters could be derived. The MPA approach was then extended to multicellular assemblies [6] like tumor spheroids [13–15], or blastocysts [16]. In the case of blastocysts, MPA can be seen as a single cell mechanical assay since only one protruding cell in connection with the other cells of the embryo is probed. By contrast, spheroids are generally treated as droplet of soft material in a framework of continuum rheology. In this context, the MPA technique is primarily used to measure apparent surface tensions and viscoelasticity at multicellular scale. Given the wide range of possibilities to vary experimental conditions (aspiration step, rate, magnitude of aspiration at steady state, relaxation upon aspiration release), and the selected phenomenological rheological model chosen, data emerging from seemingly similar experiments may lead to discrepancies or different interpretations. For instance, on the basis of two previous works, similar data were interpreted as a force-dependent increase of surface tension [13] or as a deformation-dependent viscoelasticity [17]. Clearly, a common framework is needed to analyze MPA experiments on multicellular spheroids.

Mechanistic modeling approaches aiming at modeling the steady state or aspiration dynamics of the tongue, *i.e.* the fraction of tissue that enters the pipette, have been developed to assess mechanical parameters and analyze the experimental results. However, despite the relative abundance of modeling approaches ([18] and references therein), these methods are either analytical with simple elasticity or viscoelasticity hypotheses or rely on finite elements modelling by treating the cell or aggregate as a homogeneous solid-like or fluid-like material. In our opinion, the lack of in-depth characterization analysis of the samples' rheological properties mostly originates from the fact that heterogeneities at the scale of the aggregate are not taken into account. The lack of more consistent modeling approaches has been pointed out in a recent work [19] where the authors propose a mesoscopic approach to model the MPA experiment.

In our paper, we propose a mathematical approach that models the aggregate as a solution consisting of cells and medium in the cell-cell *interstitium*. The main validity hypothesis of the model is that the characteristic size of the cellular aggregate is large enough relative to the cell size to allow the aggregate to be treated as a continuum [20]. The behavior of the cell aggregate is assumed to be intrinsically non-Newtonian and characterized by a viscoelastic rheological model. The model is used to simulate the aspiration and retraction phase of a multicellular spheroid in a MPA experiment. Comparison between numerical and experimental results demonstrates that the proposed mathematical model is able to describe all dominant mechanisms at play during the aspiration and retraction phases. Our results highlight that the relevance of the conclusions of existing studies aiming at modeling MPA is strongly correlated with the assumptions made, which are most often motivated by the need for simplification. We show in particular that the assumption of a perfect non-wetting condition between the cell aggregate and the pipette has a considerable impact on the parameters identified from inverse modeling of experimental results. We also provide a physical explanation for the observed asymmetry between the aspiration and retraction steps that does not require to assume an active response of the cells, contrary to those proposed in the literature (*e.g.* see [13,17]).

The starting hypotheses and the governing and constitutive equations of the mathematical model are presented in Section 2. Then Section 3 shows how the mathematical model is implemented to simulate the aspiration and retraction phase of a cell aggregate. Results are presented and discussed in Section 4. A conclusive paragraph, Section 5, summarizes the main outcomes of the present work.

2. The mathematical model

A cell aggregate continuum has a solid-like behavior at a small strain level (∼10 %) and for relatively short solicitation times (∼seconds) and a fluid like behavior when highly deformed during a long period of time (∼hours). In our mathematical framework we model the cell aggregate as a solution to account for its bi-constituent nature (*i.e.* cells + medium in the cell–cell *interstitium*). The model is developed within the frame of a Cahn–Hilliard–Navier–Stokes formulation which allows us to consider both effects related to cell-cell adhesion energy and to the intrinsic cell aggregate visco-elasticity by means of an Oldroyd-B rheological model. The proposed model is an extended version of the one some of us have already developed [20] for modeling confined growth of encapsulated spheroids. Here, by releasing the hypothesis of a negligible convective velocity of the solution, the momentum conservation equation does not reduce to the hydro-static case. Consequently, the Cahn–Hilliard system of equations must be solved in a coupled fashion with Navier–Stokes equations. Additionally, due to the non-Newtonian behavior of the cell aggregate a reliable viscoelastic rheological model must be adopted. This modeling approach allows us to take into account that the overall viscoelastic response observed experimentally in the initial part of aspiration (and of retraction) has two counterparts: a structural viscoelastic effect that is related to surface tension and a bulk viscoelastic effect related to the intrinsic viscoelasticity of the cell aggregate. In the following, we define the bi-constituent system, then

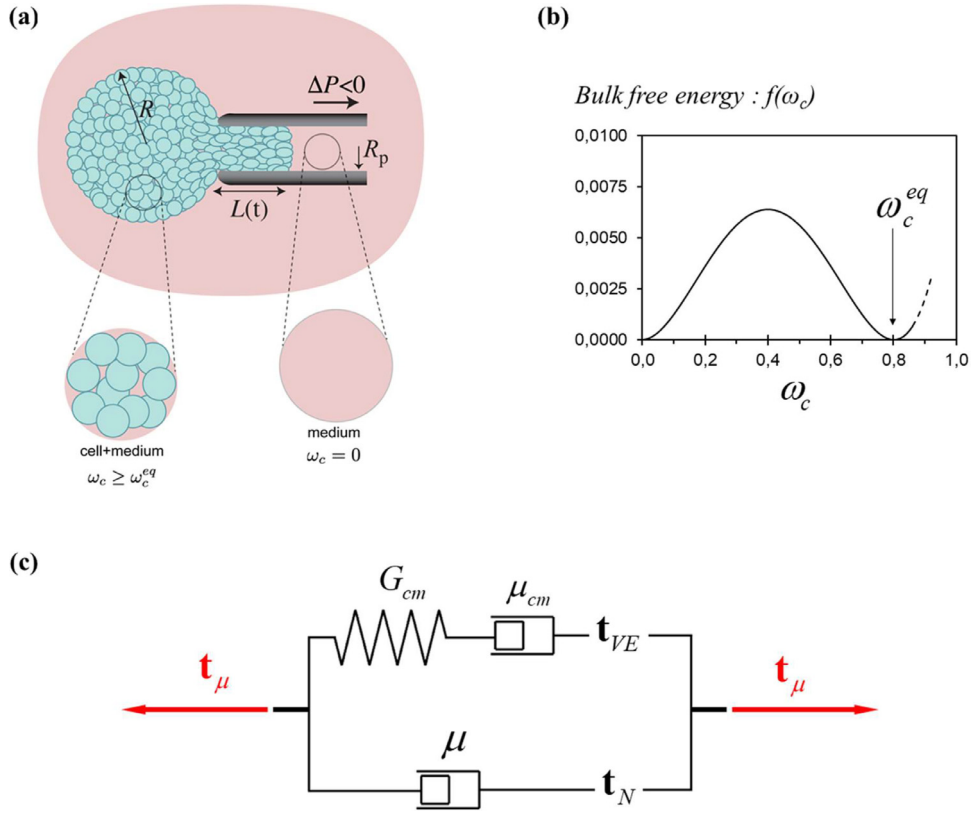

Fig. 1. Representative elementary volume (REV) for a point within the cell aggregate and in the medium (a); Bulk free energy function adopted in the Cahn–Hilliard model (b); Oldroyd-B rheological model adopted for the cell aggregate (c).

we present the governing and the constitutive equations in two respective separate paragraphs.

2.1. Definition of the bi-constituent system

The mathematical model is founded on the framework of the Thermodynamically Constrained Averaging Theory (TCAT) [21]. The starting hypothesis is that the cell aggregate must be modeled as a solution consisting of two species: the cell species, *c*, and the medium fluid species, *m*, representing the interstitial fluid present in the *interstitium* between cells. The solution may contain other chemical species in minor proportion, as oxygen for instance and other nutrients, which ensure the viability of the cells. Due to the relatively small size of the aggregate studied (diameter < 200 μm) and to the relatively short duration of the modeled experiment (∼ 5 h) we assume that the cells are well oxygenated in the whole course of the experiment; this allows us to disregard oxygen diffusion in the numerical simulations. If a representative elementary volume (REV) of solution is defined, each point of the domain can be characterized by a certain mass fraction of *c* and *m* (Fig. 1a): ω_c and ω_m respectively. Obviously, the following constraint must be respected

$$\omega_c + \omega_m = 1 \tag{1}$$

If we consider a point in the area external to the cell aggregate, the mass fraction of the medium species is the unity ($\omega_m = 1$). Conversely, if we consider a point within the cell aggregate the mass fraction of the cell species is $\geq \omega_c^{eq}$ with ω_c^{eq} the mass fraction of the cells in the cell aggregate at rest.

$$\begin{aligned} &\text{In the medium zone} : \omega_c = 0 \\ &\text{In the interface zone} : 0 < \omega_c < \omega_c^{eq} \\ &\text{In the cell zone} : \omega_c \geq \omega_c^{eq} \end{aligned} \tag{2}$$

Each point of the solution is also characterized by a certain solution velocity, $\mathbf{v}$, and by the diffusion velocities of chemical species $\mathbf{u}_i$ ($i = c, m$). The diffusion velocities are the deviations of species velocities, $\mathbf{v}_i$, with respect to the solution velocity

$$\mathbf{u}_i = \mathbf{v}_i - \mathbf{v} \qquad i = c, m \tag{3}$$

The following condition holds for diffusion velocities [21]

$$\sum_i \omega_i \mathbf{u}_i = 0 \tag{4}$$

2.2. Governing equations

Cells may move due to advective transport (related to the solution velocity $\mathbf{v}$) and diffusive transport (related to its own diffusive velocity, $\mathbf{u}_i$). As a consequence, the spatial form of the mass conservation equations of the cell species, using TCAT formalism [21], reads

$$\frac{\partial(\rho\omega_c)}{\partial t} + \nabla\cdot(\rho\omega_c\mathbf{v}) + \nabla\cdot(\rho\omega_c\mathbf{u}_c) - r_c = 0 \tag{5}$$

where ρ is the solution density and r_c is an exchange of mass term to account for chemical-biological events (*e.g.* cell division) inducing mass transfer from other species of the solution to *c* species. An analogous equation governs mass conservation of the medium species, *m*

$$\frac{\partial(\rho\omega_m)}{\partial t} + \nabla\cdot(\rho\omega_m\mathbf{v}) + \nabla\cdot(\rho\omega_m\mathbf{u}_m) - r_m = 0 \tag{6}$$

where, as in Eq. (5), r_m is a source or sink term to account for mass exchange between species. Since mass created in one species (for example in the *c* species due to cell division) has to come from other species, the following constraint must be respected

$$r_c + r_m = 0 \tag{7}$$

Table 1
Summary of the model independent variables.

Species	index	Associated variables	Equivalent scalar variables
Cells	c	ω_c, r_c, $\mathbf{u}_c$, $\mathbf{v}_c$	8
Medium	m	ω_m, r_m, $\mathbf{u}_m$, $\mathbf{v}_m$	8
Solution	–	ρ, p, $\mathbf{v}$, $\mathbf{t}_N$, $\mathbf{t}_{VE}$, $\mathbf{b}$	20
		Tot. number of scalar unknowns	36

Summing mass conservation equations of the two species of the solution (c and m), and accounting for constraints (1), (4) and (7) give the mass conservation equation of the solution as

$$\frac{\partial \rho}{\partial t} + \nabla \cdot (\rho \mathbf{v}) = 0 \tag{8}$$

The solution behavior has also to obey to its momentum conservation equation

$$\rho \frac{\mathrm{D}\mathbf{v}}{\mathrm{D}t} = \nabla \cdot \mathbf{t} + \mathbf{b} \tag{9}$$

where $\frac{\mathrm{D}\mathbf{v}}{\mathrm{D}t} = \frac{\partial \mathbf{v}}{\partial t} + (\mathbf{v} \cdot \nabla)\mathbf{v}$ is the total time derivative of the velocity vector, $\mathbf{b}$ is the volumetric force and $\mathbf{t}$ is the stress tensor. The stress tensor, $\mathbf{t}$, consists of the pressure contribution, p, and the stress contribution related to fluid viscosity: $\mathbf{t} = -p\mathbf{1} + \mathbf{t}_\mu$. Due to the non-Newtonian nature of the cell aggregate, $\mathbf{t}_\mu$ consists of a Newtonian stress counterpart, $\mathbf{t}_\mathrm{N}$, and a viscoelastic stress counterpart: $\mathbf{t}_\mathrm{VE}$, $\mathbf{t}_\mu = \mathbf{t}_\mathrm{N} + \mathbf{t}_\mathrm{VE}$. Note that the viscoelastic counterpart only exists when $\omega_c > 0$.

2.3. Constitutive equations

In the previous subparagraph the equivalent of 16 scalar independent equations have been presented:

- The scalar constraint on mass fractions (1).
- The definition of the species diffusive velocities (3) (corresponding to 6 scalar equations).
- The constraint on the diffusive velocities (4) (corresponding to 3 scalar equations).
- The scalar mass conservation equation of cells (5).
- The scalar constraint on the reaction terms (7).
- The scalar mass conservation equation of the solution (8).
- The momentum conservation equation of the solution (9) (corresponding to 3 scalar equations).

Note that the mass conservation equation of the medium species (Eq. (6)) is not included in the previous list, since it can be obtained combining Eqs. (5) and (8) (in other words it is not linearly independent).

The total number of independent variables is 36 (Table 1), consequently 20 scalar equations are needed for model closure. These 20 scalar equations correspond to 6 closure relationships which are reported in the following paragraphs.

The viscoelastic rheological model (12 scalar equations). The medium species is modeled as a Newtonian fluid of dynamic viscosity μ_m, while an Oldroyd-B model is used to account for the intrinsic viscoelastic behavior of the cell aggregate. Indeed, the cell-medium solution is a "structured fluid" for which we may define an overall stress tensor which can be expressed from the contributions of the stress of constituents (as done in porous media mechanics where we define the effective stress tensor) or from the contribution of different mechanisms as we have done here. In the adopted Oldroyd-B rheological model, widely used to model polymer solutions, we have two branches associated to two strain mechanisms acting in parallel (see Fig. 1c). The fact that the two strain mechanisms are in parallel is very important because if one mechanism is fully blocked, nothing moves. The first and second strain mechanisms are depicted in Figure SI1.a in the supplementary material.

The first strain mechanism associated to the parameter μ is representative of the overall cell aggregate fluidity which depends on the cell size, cell arrangement (number of contact interfaces) and the mass fraction of the *interstitium*. This deformation mechanism is associated to the Newtonian counterpart of the viscous stress, $\mathbf{t}_\mathrm{N}$.

The second strain mechanism is associated with the strength of cell-cell adhesion proteins, modeled by means of the parameter μ_{cm}, and elasticity (provided by the cell membrane and adhesion proteins) modeled by means of the parameter G_{cm}; strain rates associated to breakage of adhesion proteins and elastic deformation add up (to equal the strain rate of the first mechanism) and are both driven by the viscoelastic counterpart of the stress, $\mathbf{t}_\mathrm{VE}$.

The Oldroyd-B model allows to model liquids for which the overall viscosity increases with time for a constant stress (see Figure SI1.b). We now discuss three particular cases depicted in Figure SI1.c which allow to further understand the behavior.

1. When bonds between cell adhesion proteins are infinitely strong, the parameter μ_{cm} goes to ∞, the rheological model becomes a Kelvin-Voight cell and the behavior is that of a solid-like viscoelastic medium.
2. When the cell and proteins are rigid the parameter $\mathrm{G_{cm}}$ goes to ∞, the two viscosities simply add up and the behavior is that of a Newtonian fluid of dynamic viscosity $\mu_\mathrm{cm} + \mu$.
3. Finally, when μ tends to ∞, the overall fluidity is null and nothing moves because one mechanism of the two in parallel branches of the Oldroyd-B rheological model is fully blocked.

According to these definitions and hypotheses the stress tensor of the solution reads

$$\mathbf{t} = -p\mathbf{1} + \mu\left[\nabla\mathbf{v} + \left(\nabla\mathbf{v}\right)^T\right] + \mathbf{t}_{VE} \tag{10}$$

Where, $\mathbf{t}_{VE}$ is the viscoelastic extra-stress and, introducing the parameter μ_c for the contribution of cells, the Newtonian viscosity of the solution, μ, reads

$$\mu = \omega_c\mu_c + (1-\omega_c)\mu_m \tag{11}$$

To ensure that $\mathbf{t}_{VE}$ vanishes in the medium areas (where $\omega_c = 0$), similarly to the approach used in [22] we modify the classical Oldroyd-B equation as follows

$$\mathbf{t}_{VE} + \omega_c\lambda_{cm}\mathbf{t}_{VE}^{\nabla} = \omega_c\mu_{cm}\left[\nabla\mathbf{v} + \left(\nabla\mathbf{v}\right)^\mathrm{T}\right] \tag{12}$$

where $\lambda_{cm} = \mu_{cm}/G_{cm}$ and the symbol ∇ denotes the frame invariant upper-convective derivative of a tensor field which is defined as

$$\mathbf{t}_{VE}^{\nabla} = \frac{\partial \mathbf{t}_{VE}}{\partial t} + \mathbf{v}\nabla\mathbf{t}_{VE} - \left(\nabla\mathbf{v}\right)^\mathrm{T}\mathbf{t}_{VE} - \mathbf{t}_{VE}\nabla\mathbf{v} \tag{13}$$

Hence, the 2 relationships (10) and (12) can be solved in the whole domain since they give a Newtonian behavior where $\omega_c = 0$ and a viscoelastic behavior elsewhere.

The equation for the diffusive velocity of the cell species (3 scalar equations). The diffusion of the cell species is driven by the

product of the cell mobility M and the gradient of the chemical potential, ϕ,

$$\omega_c \mathbf{u}_c = -M\nabla\phi \tag{14}$$

A diffuse interface approach is used to track the interface between the cell aggregate and the medium. The interface's thickness and the composition profile through the interface are set by the competition between individual motion and reciprocal attraction/repulsion of cells which are accounted in the expression of the chemical potential, ϕ

$$\phi = \frac{\alpha\sigma}{\varepsilon} f'(\omega_c) - \alpha\sigma\varepsilon\Delta\omega_c \tag{15}$$

where the function $f(\omega_c)$, bulk free energy density of the solution, as some of us proposed in [20], has the following form

$$f(\omega_c) = \frac{1}{4}\omega_c^2\left(\omega_c^{eq} - \omega_c\right)^2 \tag{16}$$

The equilibrium value, ω_c^{eq}, is set at the density of cells in a suspended cell aggregate at rest. The assumed form of bulk free energy density has two minima one at $\omega_c = 0$, the other at $\omega_c = \omega_c^{eq}$ (Fig. 1b). In Eq. (15), σ is the cell aggregate surface tension, α and ε are a normalization coefficient to recover Young-Laplace law ($\alpha = \frac{6\sqrt{2}}{(\omega_c^{eq})^3}$) and a measure of the interface thickness respectively [20].

The expression of the volumetric force (3 scalar equations). The body force in Eq. (9), which allows to account for the pressure difference between the medium and the cell aggregate, is given by the chemical potential, ϕ, times the gradient of cells mass fraction, ω_c [20]

$$\mathbf{b} = \phi\nabla\omega_c \tag{17}$$

The state equation for the solution density (1 scalar equation). We assume here that the bulk species (medium and cell species) are incompressible, which implies that their solution is also incompressible. However, the density of the solution, ρ, generally depends on its composition. As explained in Section 3.3 *'Physical Parameters'*, the densities of the cell and medium species, ρ_c and ρ_m, are very similar and can therefore be considered equal. Since $\rho_c = \rho_m$, the density of the solution, ρ, is equal to the density of the bulk species and can be assumed constant.

$$\rho = \rho_0 \tag{18}$$

The expression of one of the two reaction terms (1 scalar equation). In the modeled examples we assume the cell in homeostasis so r_c is zero (consequently also r_m is zero, *see* Eq. (7)).

2.4. Final form of the governing equations and boundary conditions

The density of the solution ρ is constant [*cf.*Eq. (18)] so Eq. (8) reduces to the divergence free equation (as in the Boussinesq approximation). We introduce here the further assumption that, given the orders of magnitude of inertial *versus* viscous forces in the micropipette aspiration experiment [13], the Reynolds number of the problem is very low. This allow us to neglect the term $(\mathbf{v}\cdot\nabla)\mathbf{v}$ in the total derivative of Eq. (9) which reduces to the partial derivative with respect to time. Taking into account this assumption and accounting for the previously presented constitutive relationships, the final form of the system of Partially Differential Equations (PDEs) reads

$$\frac{\partial\omega_c}{\partial t} + \nabla\cdot(\omega_c\mathbf{v}) - \nabla\cdot\left(M\nabla\phi\right) = 0 \tag{19}$$

$$\phi = \frac{\alpha\sigma}{\varepsilon} f'(\omega_c) - \alpha\sigma\varepsilon\Delta\omega_c \tag{20}$$

$$\nabla\cdot\mathbf{v} = 0 \tag{21}$$

$$\rho_0\frac{\partial\mathbf{v}}{\partial t} = \nabla\cdot\left\{-p\mathbf{1} + \mu\left[\nabla\mathbf{v} + \left(\nabla\mathbf{v}\right)^T\right] + \mathbf{t}_{VE}\right\} + \phi\nabla\omega_c \tag{22}$$

$$\mathbf{t}_{VE} + \omega_c\lambda_{cm}\left[\frac{\partial\mathbf{t}_{VE}}{\partial t} + \mathbf{v}\nabla\mathbf{t}_{VE} - \left(\nabla\mathbf{v}\right)^{\mathrm{T}}\mathbf{t}_{VE} - \mathbf{t}_{VE}\nabla\mathbf{v}\right] = \omega_c\mu_{cm}\left[\nabla\mathbf{v} + \left(\nabla\mathbf{v}\right)^{\mathrm{T}}\right] \tag{23}$$

The primary variable of the system of PDE are: the mass fraction of the cell species, ω_c, the chemical potential, Φ, the velocity vector, $\mathbf{v}$, the pressure of the solution, p, and the viscoelastic counterpart of the stress tensor, $\mathbf{t}_{VE}$.

The boundary conditions related to the Cahn–Hilliard (CH) part [Eqs. (19) and (20)] allow us to model the relative wettability of the two fluid with respect of the whole bound or part of it. More precisely if the cell aggregate does not wet (or wet) the bound, a Dirichlet boundary condition prescribing $\omega_c = 0$ (or $\omega_c = \omega_c^{eq}$) must be applied. Conversely in the case of a partial wettability a Neumann condition fixing the wetting angle θ_s must be applied as done in [23]. If we call Γ_D the non-wetting (or wetting) portion of the boundary and Γ_N the partially wet one (with $\Gamma_D \cup \Gamma_N = \Gamma$), the two types of boundary conditions read

$$\omega_c = \omega_0 \qquad \text{on} \quad \Gamma_D \tag{24}$$

$$\mathbf{n}\cdot\nabla\omega_c = -\cot\left(\theta_s\right)\left|\boldsymbol{\tau}\cdot\nabla\omega_c\right| \qquad \text{on} \quad \Gamma_N \tag{25}$$

For the chemical potential in the presented examples, we set a natural condition on the whole boundary

$$\mathbf{n}\cdot\nabla\phi = 0 \qquad \text{on} \quad \Gamma \tag{26}$$

which ensures that the cells do not diffuse through impermeable surfaces.

For the Navier–Stokes (NS) part of the model [Equs. (21) to (23)] two types of boundary conditions can be applied: either the velocity vector (or some of its components) is prescribed either a traction condition is applied. In the following, we will assume that in the portion of the boundary, Γ_t, where we assume a traction condition the traction vector has not tangential component. The other part of the boundary where we set the velocity vector is indicated as Γ_v . Hence the boundary conditions for the NS equations read

$$\mathbf{v} = \mathbf{v}_0 \qquad \text{on} \quad \Gamma_v \tag{27}$$

$$\mathbf{t}\cdot\mathbf{n} = -p_0\mathbf{n} \qquad \text{on} \quad \Gamma_t \tag{28}$$

3. *In silico* modeling of MPA

The mathematical model is now applied to simulate MPA of a cell aggregate. Two cases are analyzed. In the first one, as generally assumed to interpret experimental data, we consider a non-wetting situation between the pipette walls and the cells (contact angle θ_s =180°); in the second case we assume a partial wetting condition with a static angle θ_s = 150° with no hysteresis.

3.1. The reference experimental test

This numerical study is based on the experimental results published by one of us in Guevorkian *et al.* [13]. In this paper the authors propose the use of the MPA technique to study the surface tension and mechanical properties of cell aggregates. Due to its viscoelastic properties when the cell aggregate is aspirated, it initially responds as an elastic solid, then as a viscous fluid at times larger than a certain characteristic time of about few tens of min. The micropipette has been chemically treated to limit the adhesion

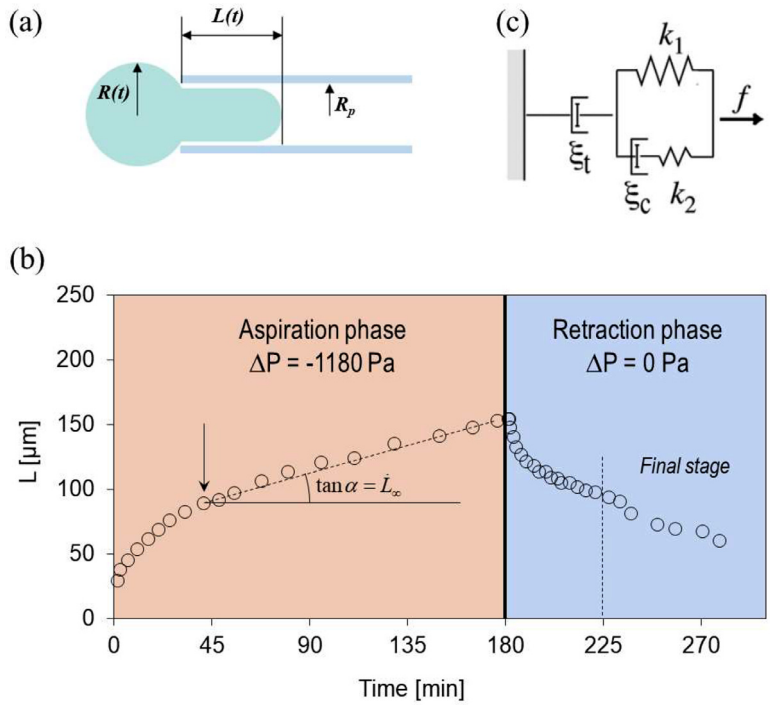

Fig. 2. (a) Geometrical description of the MPA test; (b) Experimental results for the aspiration and retraction phases of the modeled case. $\dot{L}_\infty$ characterizes the viscous flow; (c) Rheological model adopted for the analytical solution proposed in [13] where k_1 and k_2 are the spring constants and ξ_c and ξ_t are the dashpots corresponding to the modified Maxwell model.

of cells to the internal wall of the pipette, leading to the assumption of a 180° contact angle. During the experiment, the aspiration of the aggregate in the pipette of radius R_p was monitored by tracking the position $L(t)$ of the end of the tongue (Fig. 2a). In the simulated example $R_p = 35$ μm while the initial radius of the cells aggregate (just before aspiration) is $R_{(0)} = 175$ μm. A suction pressure $\Delta p = -1180$ Pa has been applied within the pipette during 180 minutes to aspirate the aggregate and monitor the advancement of the tongue; then the pressure Δp has been set to zero which leads the retraction of the aggregate. During the aspiration phase after a fast initial deformation (elastic phase) the advancement of the front reaches a quite constant velocity as shown in Fig. 2b. The behavior is similar in the initial stage of the retraction phase; then in the final stage of the retraction the behavior slightly evolves (see data points in Fig. 2b after 225 min). An analytical solution based on a 1D rheological model (different from the Oldroyd-B proposed here, *cf.* Fig. 2c *versus* Fig. 1c) has been adopted in [13] to simulate this experiment. This solution gives $L(t)$ as:

$$L(t) = \frac{f}{k_1}\left(1 - \frac{k_2}{k_1 + k_2} e^{-\frac{t}{\tau_c}}\right) + \frac{f}{\xi_t} t \tag{29}$$

where f is the aspiration force and τ_c is the characteristic time of the elastic regime; the relationships between the parameters of the rheological model and the physical and geometrical properties of the experimental system are reported in [13]. As observed from the experimental data points, the retraction phase has an overall dynamics faster than the aspiration dynamics. This behavior has been related to the increase of cell surface tension during the aspiration phase. The hypothesis of a stress dependent surface tension related to the augmentation of tissue cohesion upon the application of a permanent external load is the signature of a mechano-active process. In a more recent article [17], similar experiments have been performed, and the authors suggested a further generalization of the mechano-active process assuming that the viscoelasticity of cells is deformation dependent. Since the proposed mathematical model accounts for pseudo-elastic effect related to surface tension and bulk viscoelesticity, we wish to examine if we can explain these data and appreciate the dominant effect without *a priori* hypotheses.

3.2. Boundary conditions

To reduce the computational cost of the numerical simulations we have exploited the cylindrical symmetry of the problem (Fig. 3a). The boundary conditions for NS and CH equations are depicted in Fig. 3b.

For the NS system, we have four types of boundary conditions for the four bounds B1, B2, B3 and B4:

- On B1 a normal stress equal to 0 Pa is set.
- On B2 which corresponds to the surface of the pipette the velocity vector is set null (no-slip condition).
- On B3 which corresponds to the right extremity of the pipette we set the suction pressure ($p_0 = 1180$ *Pa* which corresponds to that applied experimentally) during 180 minutes (aspiration phase) then we set $p_0 = 0$ *Pa* (retraction phase).
- On B4 the axial-symmetry of the problem is accounted by setting the velocity component $v_r = 0$.

For the CH system we shall distinguish the boundary conditions for the two cases, *i.e.* the non-wetting and the partial wetting case.

For the non-wetting case:

- On the boundary B1 U B2 U B3 a natural condition is assumed for the chemical potential while a non-wetting condition is assumed for the mass fraction of cells.
- On B4 the boundary condition respects the axial-symmetry of the problem [natural conditions (null normal gradient) are assumed for both the chemical potential and the mass fraction of cells].

For the partial wetting case:

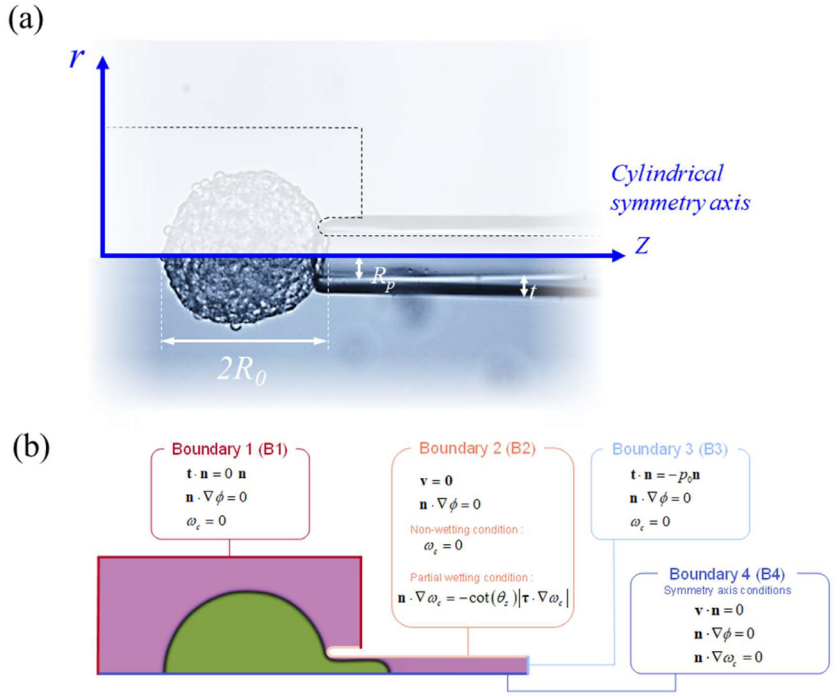

Fig. 3. Axial-symmetrical configuration of the modeled case (a); Boundary conditions (b).

Table 2
Parameters of the mathematical model for cell aggregate aspiration–retraction.

Parameter	*Symbol*	value	unit	Source
Equilibrium value of cell mass fraction	ω_c^{eq}	0.8	-	[20,24]
Density of the medium	ρ_m	1000.	kg/m^3	[20] DMEM
Dynamic viscosity of the medium	μ_m	1600.	Pa.s	Assumed as hypothesis
Density of the of cells	ρ_c	1000.	kg/m^3	[25–28]
Non wetting assumption				
Interfacial tension between the cell and the medium	σ	0.0092	N/m	Identified in this study
Elasticity coefficient of the rheological Oldroyd-B model	G_{cm}	14.7	Pa	Identified in this study
Deformation-driven viscosity of the rheological Oldroyd-B model	μ_{cm}	3.91 × 10^5	Pa.s	Identified in this study
Newtonian viscosity of the cell species in the Oldroyd-B model	μ_c	0.51 × 10^5	Pa.s	Identified in this study
Mobility of the *cm* interface	M	2.09 × 10^{-16}	m^5 s^{-1}J^{-1}	Identified in this study
Partial-wetting assumption				
Interfacial tension between the cell and the medium	σ	0.0099	N/m	Identified in this study
Elasticity coefficient of the rheological Oldroyd-B model	G_{cm}	19.2	Pa	Identified in this study
Deformation-driven viscosity of the rheological Oldroyd-B model	μ_{cm}	1.02 × 10^5	Pa.s	Identified in this study
Newtonian viscosity of the cell species in the Oldroyd-B model	μ_c	0.17 × 10^5	Pa.s	Identified in this study
Mobility of the *cm* interface	M	3.80 × 10^{-16}	m^5 s^{-1} J^{-1}	Identified in this study

- The conditions are the same as for the non-wetting case with exception on the surface of the pipette (B2) where a condition of partial wetting is applied.

The cell aggregate is initially outside the pipette. Then, thanks to the suction pressure applied on B3, it starts to be aspirated during 180 min. After 180 min the pressure on B3 is set null so the aggregate starts to retract until it fully exits the pipette. The physical parameters used in the mathematical model are summarized in the Table 2.

3.3. Physical parameters

To run the mathematical model, we need to set some parameters. The parameter ω_c^{eq} in Eq. (16) corresponds to the homeostatic cell compactness which is directly correlated with the inter-cellular space density (cell compactness = 1. – inter-cellular space density). The inter-cellular space density can be quantified through various imaging techniques such as high-resolution transmission electron microscopy (TEM), which provides detailed internal cellular organization information. In the micro-pipette experiment modeled in our work, the inter-cellular space density was not evaluated, so we decided to assume $\omega_c^{eq} = 0.8$ which is in the right range of value which can be found in the literature. For example, in [24] the authors measured an inter-cellular space density of around 0.14 (14 %) in the viable rim of the analyzed cell aggregates, which corresponds to a compactness of around 0.86.

We focus now on the densities of the two species of the two-constituent system, ρ_m and ρ_c. The medium used in the experiment is a Dulbecco's Modified Eagle Medium (DMEM) which is primarily an aqueous solution with small amount of salts, and proteins. Its mass density is therefore very close to that of water, so in the mathematical model we assume $\rho_m = 1000$ kg/m^3. Focusing now on the cell species, the typical mass density of a mammalian cell is approximately 1050 kg/m^3, *e.g.* see [25,26], and it only slightly varies by less than 1 % around this value [27] depend-

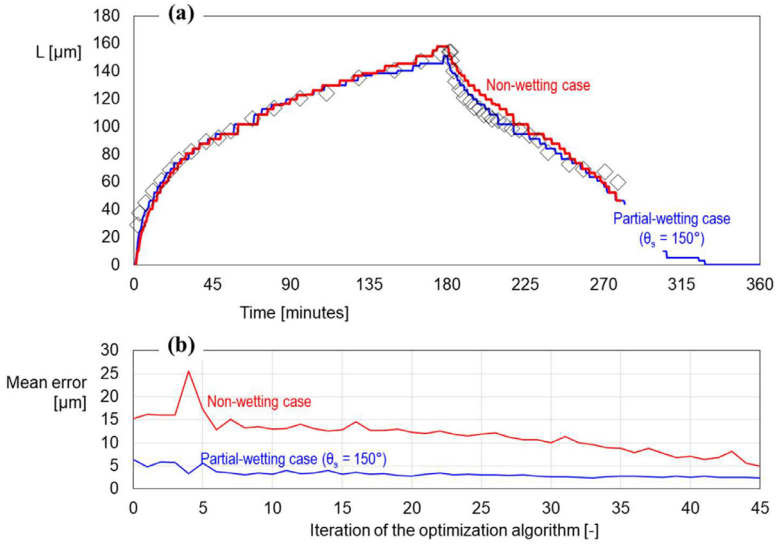

Fig. 4. Identification of the input parameters for non-wetting (red) and partial-wetting (blue) cases: experimental results *versus* numerical results (a); convergence of the optimization algorithm (b).

ing on the cell types (size of the nucleus compared to cytoplasm) or physiological state in the division cycle [28]. The density of the cell species, ρ_c, is therefore also taken equal to 1000 kg/m^3. The fact that $\rho_c = \rho_m$ as anticipated in Section 2.4 allows us to simplify the final form of the governing equations implemented in the finite element code.

Considering now the viscosity of the medium species, due to the huge difference between it and the dynamic viscosity of the cell (at least 8 orders of magnitude), we experienced some convergenece issues in the numerical solution. To overcome this problem, we studied the influence of the medium viscosity μ_m and we observed that, for a given μ_c, when $\mu_m < 2000$ Pa.s the sensitivity of the solution to the medium viscosity becomes negligible compared to that of μ_c and that of the other input parameters. This analysis reported in Fig. SI2 allows us to use a value of μ_m which is significantly higher than the real one and therefore enable the convergence of the numerical analysis (we used in particular $\mu_m = 1600$ Pa.s).

While ω_c^{eq} ρ_m μ_m and ρ_c are *a priori* fixed, all the other parameters are identified by inverse modeling. As we consider two cases (*i.e.* non wetting and partial wetting conditions) Table 2 reports the set of parameters finally identified in the two situations.

3.4. Spatial and temporal discretization of the equation

The governing equation of the model are discretized in space and in time with Finite Elements (FE) and Finite Differences (FD) respectively. The model is implemented in the open-source finite element platform *Fenics* (the codes are available on Github, at https://github.com/gsciume/Cahn-Hilliard-Navier-Stokes) accounting for the axial symmetry of the problem to suitably model its three-dimensional nature.

The nonlinear system of equations has been solved adopting a Newton algorithm for which we set a relative tolerance of 1×10^{-6} and a maximum number of 30 iterations. A fine mesh is generated in the area where we expect the presence of the aggregate-medium interface while a coarser mesh is used in the other parts of the domain.

Preliminary sensitivity analyses have been performed to select the suitable time step and characteristic size of the finite element mesh which are $dt = 10$ s and $dh = 5$ μm respectively. We also studied the convergence with respect to the parameter ε in Eq. (20) which controls the thickness of the interface between the medium and the cell aggregate. Fig. SI3 in the supplementary material shows that when $\varepsilon \leq 1.4$ μm the numerical solution becomes almost insensitive to the parameter. Hence, we set $\varepsilon = 1.4$ μm.

4. Results and discussion

In this section we first explain the methodology used to identify the physical parameters of the model and comment on the differences in the set of parameters obtained for the two considered scenarios (*i.e.* non-wetting and partial wetting conditions). Then a sensitivity study is presented to evaluate how much the mathematical model is sensitive to its governing parameters. Finally, an in-depth analysis of the flow pattern, pressure and chemical potential distribution are provided to better decipher the physics at play.

4.1. Identification of the input parameters

To identify the input parameters the Nelder–Mead method has been used exploiting the constrained minimization algorithm *optimize.minimize* implemented in the free and open-source Python library *Scipy*. This algorithm has been used to minimize the root-mean-square deviation (RMSD) between the numerical and experimental results for the evolution of $L(x)$ over time.

Five parameters have been optimized namely: the parameters μ_{cm}, G_{cm} and μ_c of the rheological Oldroyd-B model, the interfacial tension between the cell and the medium, σ, and the mobility parameter, M. The initial guess vector [μ_{cm}, G_{cm}, μ_c, σ, M] for the no wetting and partially wetting cases are respectively: [150 kPa.s, 20 Pa, 50 kPa.s, 0.01 N/m, 4×10^{-16} m^{5}s^{-1}J^{-1}] and [75 kPa.s, 20 Pa, 20 kPa.s, 0.01 N/m, 4×10^{-16} m^{5}s^{-1}J^{-1}]. These initial guess parameters for the two cases have been selected accounting for the order of magnitude of the physical parameter identified in the reference experiment by one of us [13]. Thanks to some preliminary numerical analyses, we have also taken into account that in the no wetting case for a given overall aspiration-retraction dynamics to fit the experimental results the fluid must be more viscous than in the partially wetting case.

The advancement of the aggregate $L(t)$ obtained with the optimized set of parameters for the two cases is reported in Fig. 4a together with the experimental results.

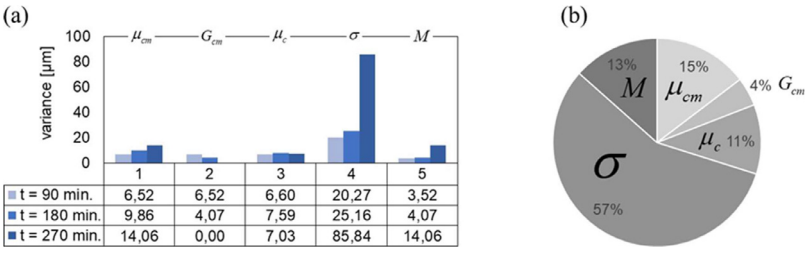

	1	2	3	4	5
t = 90 min.	6,52	6,52	6,60	20,27	3,52
t = 180 min.	9,86	4,07	7,59	25,16	4,07
t = 270 min.	14,06	0,00	7,03	85,84	14,06

Fig. 5. Sensitivity analyses: Difference in the solution at different time stages when perturbing by 30 % (one by one) the 5 selected parameters (a); overall sensitivity of the solution (b).

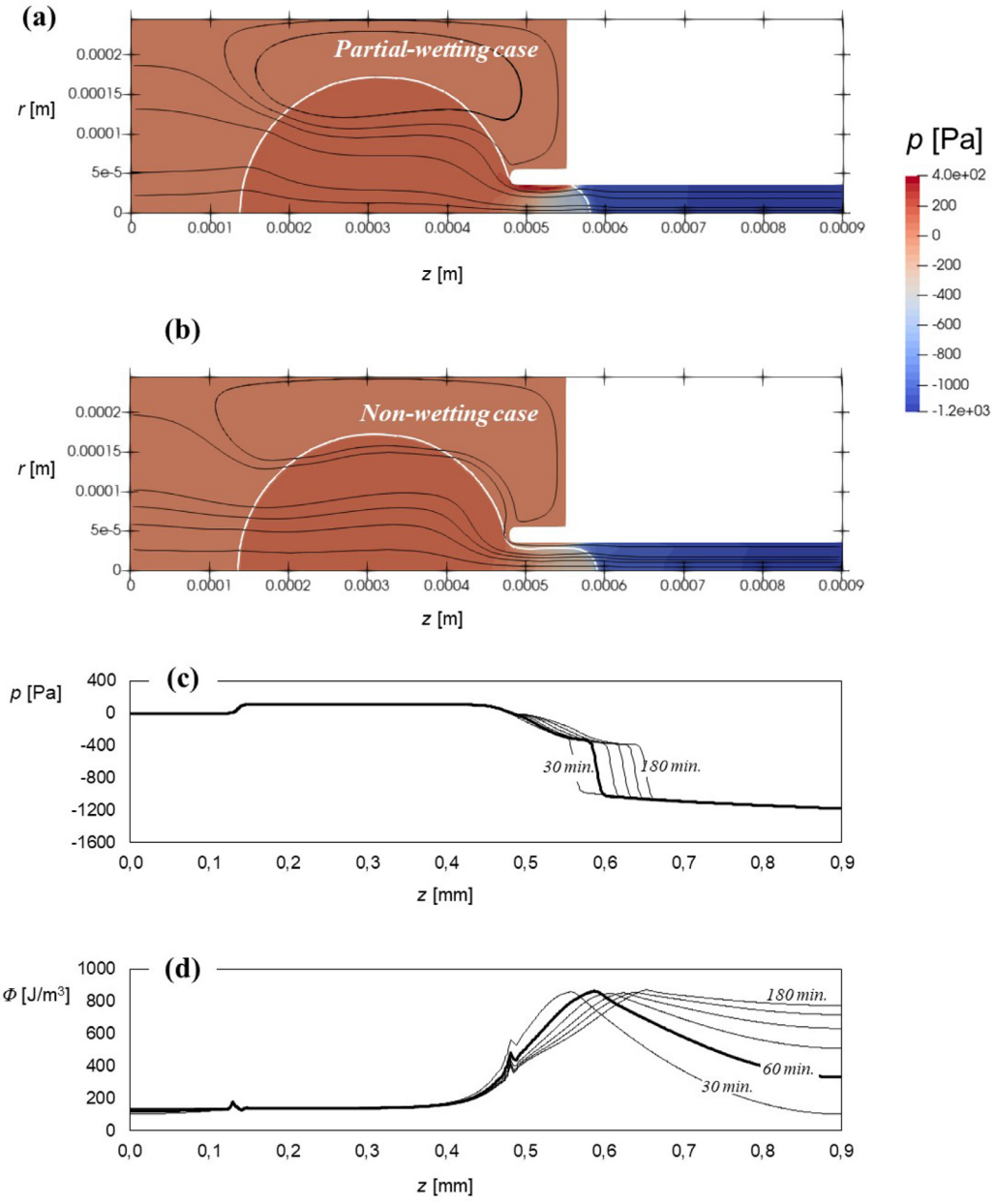

Fig. 6. Pressure distribution and stream lines after 60 min of aspiration for the partial-wetting (a) and the non-wetting (b) cases; Pressure (c) and chemical potential (d) potential profiles over the z axis at different times (each 30 min) for the non-wetting case during the aspiration phase (0–180 min).

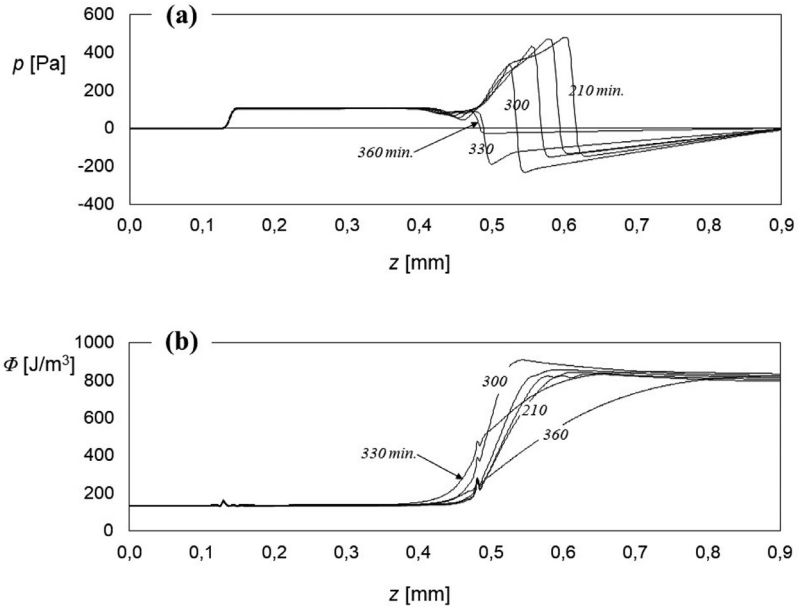

Fig. 7. Pressure (a) and chemical potential (b) potential profiles over the z axis at different times (each 30 min) for the non-wetting case during the retraction phase (180–360 min).

Fig. 4b shows how the RMSD decrease with the iterations of the optimization algorithm. We launched the optimization algorithm in parallel for the wetting and non-wetting cases by setting conditions on the maximum acceptable mean error (5 μm), a minimum number of iterations (10), and a maximum number of iterations (100). As the initial guess for the partially-wetting case was already quite good, its error rapidly decreased below 5 μm. Conversely, with an initial mean error of almost 15 μm, 45 iterations were necessary for the non-wetting case to reach the acceptable mean error. At the end of the optimization process in the partial-wetting case the RMSD reduces from 6 µm to 2.5 µm while in the non-wetting case we obtain a final RMSD of 5 µm. After 45 iterations the error of the non-wetting case still had a slight downward trend, but as the solution respected the criterion on the maximum acceptable mean error we decided to not further optimize the solution.

4.2. Sensitivity analysis

To study how the solution of the model is sensible to the five identified parameters a sensitivity analysis has been performed. Only the sensitivity analysis performed for the partially wetting case is reported here, as results obtained for the non-wetting case are quite similar.

The sensibility study is a first order analysis. Strictly speaking each parameter is increased by 30 %, taking the other ones unchanged, and we evaluated the variance of the solution of the $L(t)$ curve at 90 min (mean time of the aspiration phase), 180 min (end of the aspiration phase) and 270 min (mean time of the retraction phase). The results, provided in µm, are depicted in Fig. 5a. From the histograms it is clear that the interfacial tension is the most sensible parameters and that its impact is considerable in the retraction phase. Fig. 5b provides the overall sensitivity calculated on the whole curve $L(t)$. This is calculated by computing the overall mean variance associated to the perturbation of each parameter. The variance V_e of the *e in silico* experiment is calculated with respect to a numerical reference solution as follows

$$V_e = \frac{\sum_{t=1}^{n} \sqrt{\left[L_t(\mathbf{x}_e) - L_t\left(\mathbf{x}_{ref}\right)\right]^2}}{n} \tag{30}$$

where the L_t are n discrete values of the solution at specific time points. A first-order sensitivity index, Si, is then calculated from the first order variance as

$$S_i = \frac{V_i}{V_{tot}} \tag{31}$$

Where $V_{tot} = \sum_i V_i$. The role of the interfacial tension appears as dominant also in the representation in Fig. 5b as it gathers almost the 60% of the total variance.

4.3. Pressure and chemical potential distribution

Here, we compare the solutions obtained for the partially wetting and non-wetting cases more in detail; Fig. 6a and b shows the numerical results for the pressure and stream lines (see also the pressure distribution over the full experiment duration in Video S1 and S2). The depression in the right part of the pipette leads to a net force that drives the aspiration process. The pressure and chemical potential profiles for the non-wetting case over the axis z at different times are depicted in Fig. 6c and d, for the aspiration phase, and in Fig. 7a and b for the retraction phase.

5. Conclusion

We used here digital twinning of MPA for a better interpretation of a typical MPA experiment of aspiration and retraction. First, there is a good agreement between the numerical and experimental values, both during the aspiration and retraction phase; remarkably, a sole set of parameters allows us to model both the aspiration and retraction phase. Second, examination of the numerical results reveals the subtle but important effect of wetting whose effect is more important in the case of retraction as it can be seen in Fig. 4a where partial-wetting case give slightly better prediction of experimental data.

Usually, a non-wetting condition is assumed for the sake of simplicity. Here, we show that, in the non-wetting case, during the aspiration phase, the lubrication effect of the medium wetting the internal walls of the pipette (Fig. 6b) assists the advancement of the aggregate while this lubrication effect is not present in the partial-wetting case (Fig. 6a) because the cell aggregate is

in contact with the pipette walls. This allows to explain the significant difference in the identified viscosity parameters, μ_{cm} and μ_c (Table 2) for the partial- and non-wetting cases. It also explains why the mobility parameter, M, of the partial wetting case is 80% larger than that of the non-wetting case; indeed, the cell aggregate being in contact with the inner walls of the pipette, the advancement of the triple-point where the two-fluids and the solid meet is partly controlled by the species mobility, M. Also the elasticity parameters, G_{cm}, are quite different for the two cases. We observe that the results for the viscosity and elasticity parameters have the same order of magnitude of that identified in [13] but are not directly comparable since the rheological model assumed here is different.

Focusing now on the interfacial tension, σ, our results demonstrate that σ is quite insensitive to the assumption of non-wetting or partial wetting (the difference is only of 7 %). We found a value ($\sim$10 mN/m) which is in good agreement with the one derived in [13], in the 10–25 mN/m range; however, in our case we do not need to assume a variable surface tension to model aspiration-retraction asymmetry. The mechanism inducing the aspiration-retraction asymmetry can be understood by examining Fig. 6c and d and 7a and b. During the aspiration phase, which is driven by the pressure gradient, the gradient of the chemical potential tends to mitigate the rate of the process (Fig. 6c and d). Conversely, during the retraction stage, both the pressure gradient and the gradient of the chemical potential contribute on the retraction of the cell aggregate to recover the initial spherical shape (Fig. 7a and b). These mechanisms give a physical explanation to the asymmetry of the aspiration-retraction behavior without resorting to a variable surface tension.

While these cellular aggregates are often considered as viscoelastic fluids as a first approximation, clear manifestations of activities have been evidenced, and in particular in MPA. For instance, a shivering process consisting pulsed contractions was reported [14]. This process, which is suppressed by treating the cells with a drug that inhibits contractility, is undoubtedly active. As a consequence, even though we cannot claim that surface tension does not vary, and that the whole behavior of an aspirating and retracting cell aggregate is the same as a drop of inert liquid, we propose here a comprehensive alternative analysis that holds both for living cells and for inert matter.

This proof-of-concept work, which aims at presenting the generality and capabilities of the proposed CHNS model, is inspiring for future studies. As a perspective, we plan to vary the configuration of the experiment, to propose an improved experimental metrology (e.g., measure the flow rate within the pipette, correlate cadherin expression with the identified surface tension, better assess the wetting or non-wetting property of the pipette, etc.), and to verify that our mathematical model preserves its reliability under different experimental conditions.

Declaration of competing interest

The authors declare that they have no known competing financial interests or personal relationships that could have appeared to influence the work reported in this paper.

CRediT authorship contribution statement

Giuseppe Sciumè: Writing – review & editing, Writing – original draft, Visualization, Validation, Software, Methodology, Investigation, Formal analysis, Data curation, Conceptualization. **Karine Guevorkian:** Writing – review & editing, Writing – original draft, Conceptualization. **Pierre Nassoy:** Writing – review & editing, Writing – original draft, Conceptualization.

Acknowledgments

We wish to acknowledge financial support from ANR under Grant No. ANR-23-CE45-0016 (MATISSe – MAthematical TISSues). We wish also to acknowledge Prof. William G. Gray (University of North Carolina) for the enriching discussions on the theoretical aspects of the proposed mathematical model.

Supplementary materials

Supplementary material associated with this article can be found, in the online version, at doi:10.1016/j.actbio.2024.09.043.

References

[1] CL Guo, NC Harris, SS Wijeratne, EW Frey, CH Kiang, Multiscale mechanobiology: mechanics at the molecular, cellular, and tissue levels, Cell Biosci. 3 (2013) 25.
[2] DH Kim, PK Wong, J Park, A Levchenko, Y Sun, Microengineered platforms for cell mechanobiology, *Annu. Rev. Biomed. Eng.* 11 (2009) 203–233.
[3] P Wu, D Aroush, A Asnacios, W-C Chen, ME Dokukin, BL Doss, P Durand-Smet, A Ekpenyong, J Guck, NV Guz, PA Janmey, JSH Lee, NM Moore, A Ott, Y-C Poh, R Ros, M Sander, I Sokolov, JR Staunton, N Wang, G Whyte, D Wirtz, A comparison of methods to assess cell mechanical properties, Nat. Methods 15 (2018) 491–498.
[4] R.A. Foty, G. Forgacs, C.M.Pfleger Gabo, M.S. Steinberg, Liquid properties of embryonic tissues: measurement of interfacial tensions, Phys. Rev. Lett. 72 (14) (1994) 2298–2301.
[5] H Wang, F Zhou, Y Guo, LA Ju, Micropipette-based biomechanical nanotools on living cells, Eur. Biophys. J. 51 (2022) 119–133.
[6] K Guevorkian, JL Maître (2017) Chapter 10 - micropipette aspiration: a unique tool for exploring cell and tissue mechanics in vivo in *Cell Polarity and Morphogenesis*, Methods in Cell Biology, ed. T Lecuit. Academic Press) Vol. 139, pp. 187–201.
[7] K Guevorkian, F Brochard-Wyart, D Gonzalez-Rodriguez, in: Chapter Eight - Flow Dynamics of 3D Multicellular Systems into Capillaries in *Viscoelasticity and Collective Cell Migration*, Elsevier, 2021, pp. 193–223.
[8] JM Mitchison, MM Swann, The mechanical properties of the cell surface: I. the cell elastimeter, J. Exp. Biol. 31 (1954) 443–460.
[9] EA Evans, RM Hochmuth, A solid-liquid composite model of the red cell membrane, The J. Membr. Biol. 30 (1976) 351–362.
[10] W Rawicz, K Olbrich, T McIntosh, D Needham, E Evans, Effect of chain length and unsaturation on elasticity of lipid bilayers, *Biophys. J.* 79 (2000) 328–339.
[11] K Olbrich, W Rawicz, D Needham, E Evans, Water permeability and mechanical strength of polyunsaturated lipid bilayers, Biophys. J. 79 (2000) 321–327, doi:10.1038/s41598-024-70759-y.
[12] E Evans, A Yeung, Apparent viscosity and cortical tension of blood granulocytes determined by micropipet aspiration, *Biophys. J.* 56 (1989) 151–160.
[13] K Guevorkian, MJ Colbert, M Durth, S Dufour, F Brochard-Wyart, Aspiration of biological viscoelastic drops, Phys. Rev. Lett. 104 (2010) 218101.
[14] K Guevorkian, D Gonzalez-Rodriguez, C Carlier, S Dufour, F Brochard-Wyart, Mechanosensitive shivering of model tissues under controlled aspiration, Proc. Natl. Acad. Sci. 108 (33) (2011) 13387–13392.
[15] D Gonzalez-Rodriguez, K Guevorkian, S Douezan, F Brochard-Wyart, Soft matter models of developing tissues and tumors, Science 338 (2012) 910–917.
[16] Ö Özgüç, L de Plater, V Kapoor, AF Tortorelli, A G Clark, J-L Maître, Cortical softening elicits zygotic contractility during mouse preimplantation development, PLOS Biol. 20 (2022) 1–23.
[17] RC Boot, A van der Net, C Gogou, P Mehta, DH Meijer, GH Koenderink, PE Boukany, Cell spheroid viscoelasticity is deformation-dependent, Sci. Rep. 14 (2024) 20013, doi:10.1038/s41598-024-70759-y.
[18] B González-Bermúdez, GV Guinea, GR Plaza, Advances in micropipette aspiration: applications in cell biomechanics, models, and extended studies, *Biophys. J.* 116 (2019) 587–594.
[19] Y Du, S Zhang, D Cheng, Y Liu, M Sun, Q Zhao, M Cui, X Zhao, The full model of micropipette aspiration of cells: a mesoscopic simulation, Acta Biomater. 157 (2023) 297–309.
[20] V Le Maout, K Alessandri, B Gurchenkov, H Bertin, P Nassoy, G Sciumè, Role of mechanical cues and hypoxia on the growth of tumor cells in strong and weak confinement: a dual in vitro–in silico approach, Sci. Adv. 6 (2020) eaaz7130.
[21] WG Gray, CT Miller, Introduction to the Thermodynamically Constrained Averaging Theory for Porous Medium Systems, Springer, 2014.
[22] D Mokbel, H Abels, S Aland, A phase-field model for fluid–structure interaction, J. Comput. Phys. 372 (2018) 823–840.
[23] H Ding, PDM Spelt, Wetting condition in diffuse interface simulations of contact line motion, Phys. Rev. E 75 (2007) 046708.
[24] M Madhavan, D Jaiswal, S Karlberg, A Duggan, HA Almarshad, KP Claffey, K Hoshino, Electron microscopy imaging and mechanical characterization of T47D multicellular tumor spheroids–Older spheroids reduce interstitial space and become stiffer, PLOS ONE 18 (5) (2023) e0286291.

[25] Y Zhao, HSS Lai, G Zhang, G-B Lee, WJ Li, Measurement of single leukemia cell's density and mass using optically induced electric field in a microfluidics chip, Biomicrofluidics 9 (2) (2015) 022406.
[26] Y Zhao, HSS Lai, G Zhang, G-B Lee, WJ Li, Rapid determination of cell mass and density using digitally controlled electric field in a microfluidic chip, Lab Chip 14 (22) (2014) 4426–4434.
[27] AK Bryan, VC Hecht, W Shen, K Payer, WH Grover, SR Manalis, Measuring single cell mass, volume, and density with dual suspended microchannel resonators, Lab Chip 14 (3) (2014) 569–576.
[28] S Son, A Tzur, Y Weng, P Jorgensen, J Kim, MW Kirschner, SR Manalis, Direct observation of mammalian cell growth and size regulation, Nat. Methods 9 (2012) 910–912.